ARTICLE

Making Nanoflowerbeds: Reaction Pathways Involved in the Selective Chemical Bath Deposition of ZnS on Functionalized Alkanethiolate Self-Assembled Monolayers

Peng Lu and Amy V. Walker*

Department of Chemistry and the Center for Materials Innovation, Campus Box 1134, Washington University, One Brookings Drive, St. Louis, Missouri 63130

ABSTRACT We have investigated the chemical bath deposition (CBD) of ZnS on functionalized alkanethiolate self-assembled monolayers (SAMs) using time-of-flight secondary ion mass spectrometry and scanning electron microscopy. The reaction mechanism involves both cluster-by-cluster and ion-by-ion growth. The dominant reaction pathway is dependent on both the SAM terminal group and the experimental conditions. On —COOH-terminated SAMs, two types of crystallites are observed: ~500 nm nanoflowers formed by ion-by-ion growth, and larger ~2 μm crystallites formed by cluster-by-cluster deposition. The nanoflowers nucleate at Zn^{2+}- carboxylate surface complexes. On —OH- and —CH_3-terminated SAMs, only the larger crystallites are formed. These do not adhere strongly to the SAM surface and can be easily removed. Finally, we demonstrate that under appropriate experimental conditions ZnS selectively deposits on the —COOH-terminated SAM regions of —COOH/—CH_3-patterned SAM surfaces, forming nanoscale "flowerbeds".

KEYWORDS: molecular devices · solar cells · selective deposition · chemical bath deposition · zinc sulfide · self-assembled monolayers

Over the past 20 years, there has been extensive research in nanoscale semiconductor materials.[1] Zinc sulfide is a II—VI semiconductor with a direct wide band gap, E_g = 3.65 eV (bulk),[2] a high refractive index,[3] and high transmittance in the visible range.[3] There are many applications for thin films and nanostructures of this semiconductor, including planar waveguides,[3] electroluminescent devices,[4,5] photocatalysts,[6—8] and dielectric filters.[9] The use of ZnS in optoelectronic devices, such as blue light-emitting diodes,[10—15] and photovoltaics[16,17] is well-known. Due to the toxic hazards associated with the production and use of CdS, there is interest in using ZnS to replace CdS as the "buffer layer" in photovoltaic cells.[16,17] ZnS has a larger band gap than CdS, which also leads to an enhancement of the blue response in such devices.[16] ZnS—polymer nanocomposites have been investigated for use in photonic materials[18] and polymer light-emitting diodes.[19]

A variety of methods have been employed to deposit ZnS, including H_2 plasma chemical sputtering,[20] thermal evaporation,[21,22] molecular beam epitaxy (MBE),[23] spray pyrolysis,[24,25] pulsed laser deposition,[26] chemical vapor deposition,[27—29] atomic layer deposition,[30] electrodeposition,[31—33] successive ionic layer adsorption and reaction (SILAR),[34] and chemical bath deposition (CBD).[35—47] Chemical bath deposition is an attractive technique for the deposition of semiconductors on organic thin films because it can be used at low temperatures (≤50 °C) which are compatible with organic materials. CBD is also performed under ambient pressure, making it an easy and inexpensive technique. Further, CBD can be easily adapted to large area processing.

Self-assembled monolayers (SAMs) have highly organized, well-defined structures and have a uniform density of terminal groups.[48,49] They can be patterned using a variety of techniques, including UV photopatterning,[50—53] scanning probe lithographies,[54,55] microcontact printing,[54,55] and electron-beam patterning,[56,57] to produce micro- and nanoscale structures difficult to make using conventional etching techniques. These patterned structures have been employed in applications including molecular electronics,[58,59] sensing,[60—62] production of microelectrodes,[63] and the immobilization of proteins and cells on surfaces.[64,65]

SAMs have also been employed to produce arrays of crystals, either as resists or

*Address correspondence to walker@wustl.edu.

Received for review July 12, 2008 and accepted January 07, 2009.

Published online January 20, 2009.
10.1021/nn800441y CCC: $40.75

as crystallization directing agents. SAMs have been used as resists for the electroless deposition of Ni,[66,67] the chemical vapor deposition of Cu,[68−70] Pd,[71] and Pt,[71] and the sol−gel deposition of (Pb,La)TiO_3 and $LiNbO_3$.[72] Crystal growth has also been directed using the hydrophilicity and hydrophobicity of SAMs. For example, the selective deposition of FeOOH,[73,74] $LiClO_4$,[66] and $CuSO_4$[66] from supersaturated solutions has been achieved using this approach. Perhaps the most interesting way to direct crystal growth and selective deposition is to employ chemical reactions with specific SAM terminal groups. Using the interaction of Pd^{2+} ions with pyridyl groups, Dressick and co-workers[75] selectively grew Co films on patterned SAM surfaces using electroless deposition. More recently, Walker and co-workers[76,77] have selectively deposited Mg using physical vapor deposition and alumina and aluminum using chemical vapor deposition. Dronavajjala *et al.*[78] have selectively grown polymer brushes on SAMs by surface ligation of the organometallic Pd initiator.

In this paper, we investigate the reaction pathways involved in the chemical bath deposition of ZnS on functionalized SAM surfaces using time-of-flight secondary ion mass spectrometry (TOF SIMS) and scanning electron microscopy (SEM). While there have been many studies of ZnS CBD, no definitive mechanism has been established.[35−47] We demonstrate that the growth of ZnS involves two different deposition mechanisms: cluster-by-cluster deposition and ion-by-ion growth. Further we show that the dominant deposition mechanism is dependent on the chemical functionality of the SAM terminus. On −COOH-terminated SAMs, two sizes of crystallites are observed: ~500 nm nanoflowers and ~2 μm flower-like crystallites. The larger crystallites are formed by the aggregation of ZnS colloids in solution (cluster-by-cluster deposition) and do not strongly adhere to the surface. In contrast, the ~500 nm nanoflowers are formed *via* ion-by-ion reactions on the surface and strongly adhere to it. In this process, Zn^{2+} ions initially form weak complexes with the terminal carboxylate groups. These Zn^{2+}−carboxylate surface complexes then act as nucleation sites for the ion-by-ion growth of ZnS. On $-CH_3$- and −OH-terminated SAMs, the ion-by-ion mechanism is not active and the dominant growth mechanism is cluster-by-cluster deposition, leading to the deposition of ~2 μm flower-like crystallites which do not strongly adhere to the surface. The TOF SIMS data also indicate that Zn is present at the Au/S interface after deposition on −OH- and $-CH_3$-terminated SAMs. We demonstrate that under appropriate experimental conditions ZnS can be selectively deposited on patterned $-CH_3$/−COOH-terminated SAM surfaces to create "nanoflowerbeds". In this case, ZnS nanoflowers are deposited *only* in −COOH-terminated SAM areas.

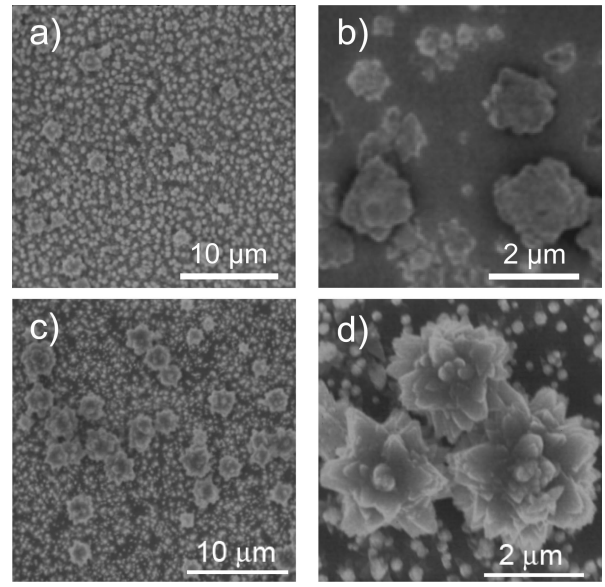

Figure 1. SEM images after ZnS chemical bath deposition for 2 h on −COOH-terminated SAM at (a,b) 22 °C and (c,d) 45 °C.

RESULTS AND DISCUSSION

ZnS Deposition on −COOH-Terminated SAMs. After ZnS CBD for 2 h, SEM images indicate that ZnS nanoflowers have deposited on −COOH-terminated SAMs, with more crystallites of both types formed at a bath temperature of 45 °C than at 22 °C (Figure 1). The chemical composition of the nanoflowers was confirmed using EDX: the nanoflowers contain only Zn and S in an approximately 1:1 ratio. In Figure 1, it can clearly be seen that there are two types of ZnS structures formed on the surface. There are many small nanoflowers, with an average diameter of 570 ± 80 nm, and larger scattered flowers, with an average diameter of 2100 ± 390 nm. In the TOF SIMS spectra, there are no molecular or cluster ions indicative of the mercaptohexadecanoic acid (MHA) monolayer, indicating that the SAM has been covered by a ZnS overlayer (see Supporting Information).

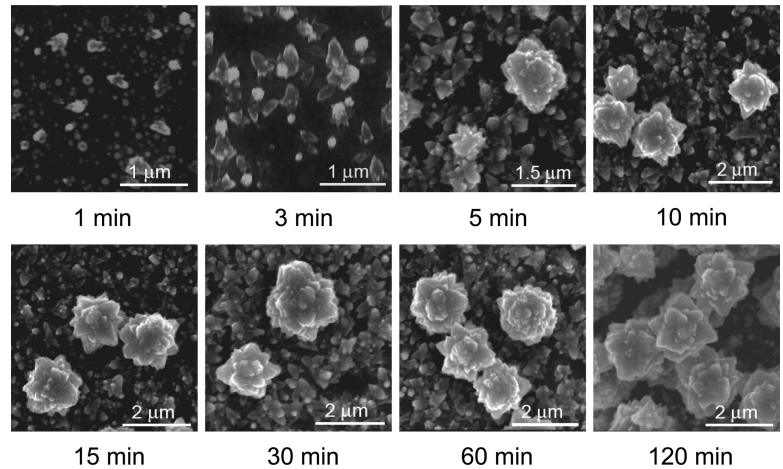

Figure 2. SEM images after ZnS chemical bath deposition on −COOH-terminated SAM at 45 °C for immersion times from 1 to 120 min.

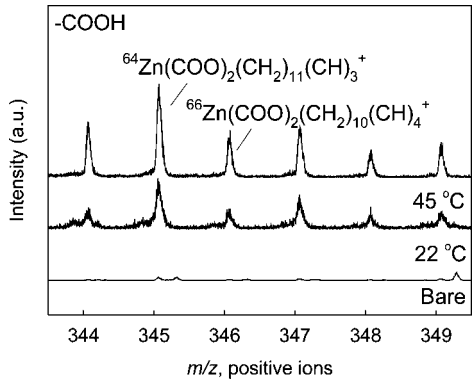

Figure 3. High mass resolution positive ion TOF SIMS mass spectra of $Zn(COO)_2(CH_2)_x(CH)_y^+$ ions ($x = 11$, $y = 3$ and $x = 10$, $y = 4$) for −COOH-terminated SAMs prior to and after ZnS chemical bath deposition for 2 h at 22 and 45 °C.

Figure 2 shows the growth of ZnS nanoflowers over time at 45 °C. After 1 min in the plating solution, we observe the formation of scattered crystallites (diameter: 50−500 nm) on the MHA surface. After 30 min, these appear to have formed a densely packed underlayer of ~500 nm ZnS nanoflowers. After 5 min, large ~2 μm flower-like crystallites are also observed on the surface. Both the size and the density of the larger crystallites increase with deposition time (see Supporting Information and Figure 5a). The crystallite diameter increases from 0.15 ± 0.07 μm after 1 min to 2.10 ± 0.39 μm after 120 min.

In the positive ion TOF SIMS spectra of the sample after 120 min CBD, $Zn(COO)_2(CH_2)_x(CH)_y^+$ ions are observed, indicating that Zn^{2+} complexes with two −COOH terminal groups (Figure 3). This observation suggests that Zn^{2+}−carboxylate complexes provide nucleation sites for the subsequent growth of ZnS nanocrystallites. There is no evidence in the TOF SIMS spectra that ZnS or Zn has penetrated through the SAM to the Au/S interface.

Our standard procedure (detailed in the Methods) is to place the −COOH-terminated SAM in a Zn^{2+} solution for 15 min prior to the addition of thiourea. This is referred to as "seeding". To investigate the importance of the complexation of Zn^{2+} with the −COOH terminal groups, we compared the nanocrystallites formed under "seeded" conditions with those formed under "unseeded" conditions, that is, when the SAM was placed directly into a plating solution containing both Zn^{2+} and thiourea ("unseeded" growth). In the former case, the Zn^{2+} ions are able to complex with the carboxylate terminal groups prior to ZnS formation, while in the unseeded case, pre-adsorption of Zn^{2+} on the SAM surface is minimized. SEM images of the resulting films are shown in Figure 4. For the seeded ZnS growth (Figure 4a), it can clearly be seen that there is a dense layer of ~500 nm nanoflowers with a few scattered, large flower-like crystallites. In contrast, for the unseeded ZnS deposition, a larger number of ~2 μm flower-like crystallites are observed than for the seeded growth,

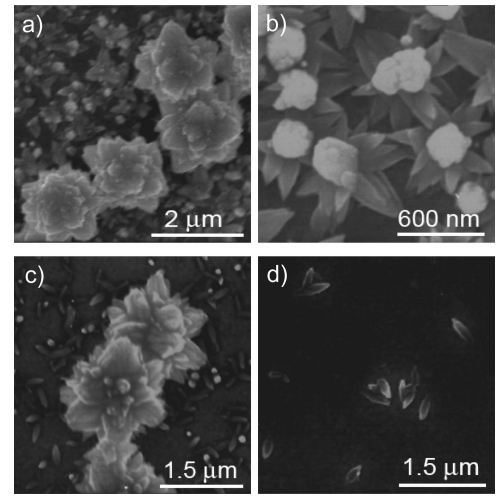

Figure 4. SEM images after ZnS chemical bath deposition at 45 °C for 2 h on −COOH-terminated SAMs under the following experimental conditions: (a) seeded deposition prior to ultrasonication; (b) seeded deposition after 5 min ultrasonication; (c) unseeded deposition prior to ultrasonication; and (d) unseeded deposition after 5 min ultrasonication. Please note that the scale bars in these images are different. The nanoflowers seen in b are the same size as the small flowers in a.

with only a few scattered ~500 nm nanoflowers (Figure 4c). We have obtained the size distributions as a function of deposition time for the growth of the large ZnS crystallites under both seeded (standard) and unseeded deposition conditions (see Supporting Information). From these, we have extracted the density of the crystallites with deposition time (Figure 5a) and the size distributions after 120 min (Figure 5b). For both seeded and unseeded reaction conditions, the number of large flower-like crystallites increases with deposition time (Figure 5a). Figure 5a also confirms that the number of large flower-like crystallites deposited is larger using the unseeded ZnS deposition conditions, by a factor of approximately two. Size distributions of the large crystallites (shown in Figure 5b and Supporting Information) are also different using seeded and unseeded ZnS deposition conditions. Under seeded conditions, the size of the crystallites increases with time from 0.15 ± 0.07 μm after 1 min to 2.10 ± 0.39 μm after 120 min, and the size distribution is relatively broad. In contrast, under unseeded conditions, the size distribution is relatively narrow (Figure 5b) and the size of the crystallites increases very slowly with time, from 1.40 ± 0.24 μm after 1 min to 1.69 ± 0.19 μm after 120 min.

Finally, the large, ~2 μm flower-like crystallites can be removed from the MHA surface by sonication of the substrate in deionized water for 5 min (Figure 4c,d). In contrast, the smaller ~500 nm nanoflowers cannot be removed using sonication, indicating that they are strongly adsorbed to the surface.

ZnS Deposition on −OH- and −CH_3-Terminated SAMs. Unlike the case of ZnS deposition on −COOH-terminated SAMs (Figure 1), SEM images indicate that no ZnS crys-

tallites form at 22 °C on −OH- and $-CH_3$-terminated SAMs (Figure 6). At 45 °C, a few ZnS crystallites are observed to form (Figure 6). However, these crystallites do not strongly adhere to the surface and can be removed by sonication in deionized water for 5 min (Figure 6).

The TOF SIMS spectra indicate that ZnS has not formed an overlayer on either the −OH- or $-CH_3$-terminated SAMs: molecular and cluster ions are observed, which are characteristic of the SAM (see Supporting Information). Further, while Zn^{2+} ions do complex with −COOH-terminated SAMs, they do not complex with the −OH and $-CH_3$ terminal groups. In the negative ion mass spectra, we also observe ions of the form $Au_xS_yZn_z^-$ (Figure 7). This indicates that Zn has penetrated through the SAM to the Au/S interface. From these data, we cannot distinguish between penetration of Zn ions and penetration of small clusters of ZnS.

Reaction Pathways of ZnS Nanoflower Deposition on −COOH-, −OH-, and $-CH_3$-Terminated SAMs. In CBD, a controlled chemical reaction is employed to deposit a thin film on a substrate by precipitation.[35] ZnS films are prepared by the decomposition of a chalcongenide, normally thiourea, in an alkaline solution containing a zinc salt and a suitable complexing agent, such as hydrazine, in the following reaction:

$$ZnL_n^{2+} + SC(NH_2)_2 + 2OH^- \rightarrow ZnS + nL + H_2CN_2 + 2H_2O$$

where ZnL_n^{2+} is a complex Zn(II) ion and L is the complexing agent. In our experiments, the complexing agent is either hydrazine or ammonia (from ammonium hydroxide).

While there have been many studies of ZnS CBD, no definitive mechanism has been established,[35−47] and the reaction pathways involved in CBD are not generally well understood.[35] Doña and Herrero[44] suggested that ZnS deposition occurs *via* the slow release and condensation of Zn^{2+} and S^{2-} ions at the surface *via* an ion-by-ion process. In contrast, Froment and Lincot[79] observed that deposited ZnS films appeared to consist of an aggregration of spherical particles. This suggested that the ZnS forms colloidal particles in solution which then deposit on the surface (cluster-by-cluster deposition).

A suitable reaction mechanism for ZnS CBD on functionalized SAMs must be able to explain the following observations: (1) Two sizes of crystallites are observed on −COOH-terminated SAMs: ~500 nm diameter nanoflowers and large ~2 μm flower-like crystallites. (2) Only large flower-like crystallites are observed on −OH- and $-CH_3$-terminated SAM surfaces. (3) The large flower-like crystallites can be removed using sonication, but the ~500 nm nanoflowers cannot. (4) A larger number of large flower-like crystallites are formed on the −COOH-terminated SAMs if the deposition is carried out under unseeded experimental conditions. (5) At 22 °C, no ZnS deposition is observed on −OH- and $-CH_3$-terminated SAMs, while at 45 °C, ZnS can be deposited on these surfaces.

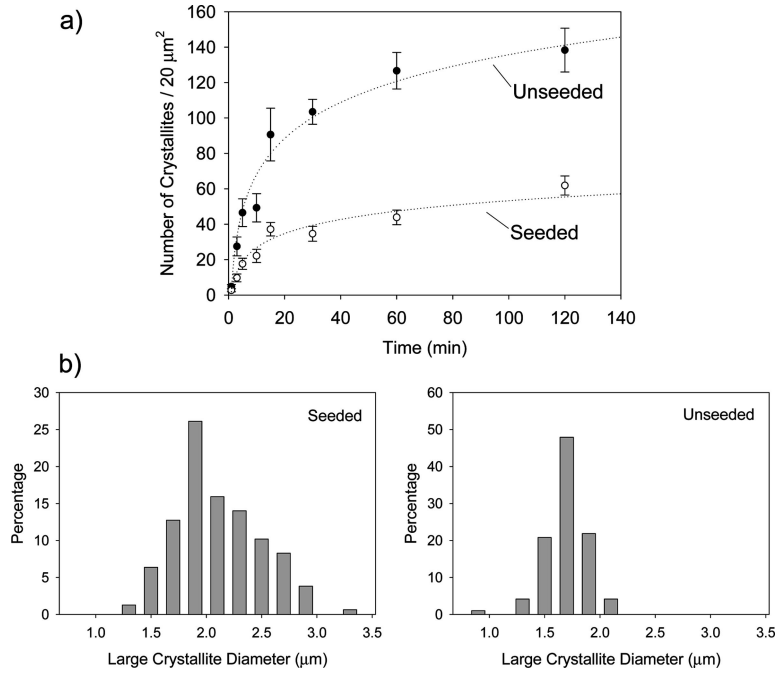

Figure 5. (a) Variation of the number of large scattered flower-like ZnS nanocrystallites with immersion time. The dotted lines are drawn as guides to the eye. (b) Size distribution of large crystallites. The width of the bars is ±0.10 μm. For seeded growth, the average diameter of the crystallite is 2.10 ± 0.39 μm, while for unseeded growth, the average diameter is 1.69 ± 0.19 μm.

We propose that ZnS nanoflowers form in the following way. Upon immersion in the plating solution, Zn^{2+} forms weak complexes with −COOH terminal groups, but not with −OH- and $-CH_3$-terminated SAMs. Since the pH of the plating solution (10−11) is higher than the pK_a of hexadecanoic (palmitic) acid (~8.5−8.8),[80] it is likely that many of the terminal groups in the −COOH-terminated SAM (MHA) are deprotonated and Zn^{2+}−carboxylate complexes can be formed. This hypothesis is supported by TOF SIMS data that suggest that zinc ions complex with two car-

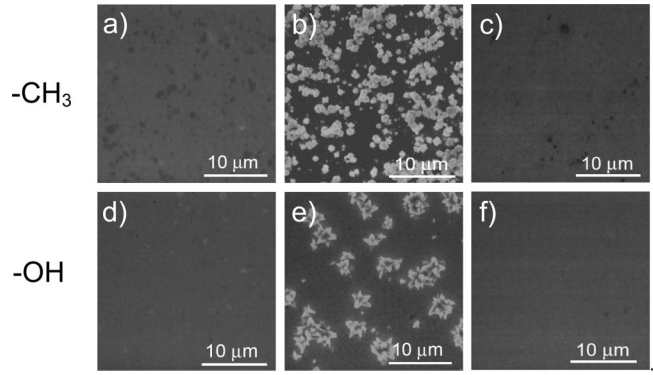

Figure 6. SEM images after ZnS chemical bath deposition for 2 h on $-CH_3$- and −OH-terminated SAMs at (a,d) 22 °C, (b,e) 45 °C, and (c,f) 45 °C after ultrasonication for 5 min.

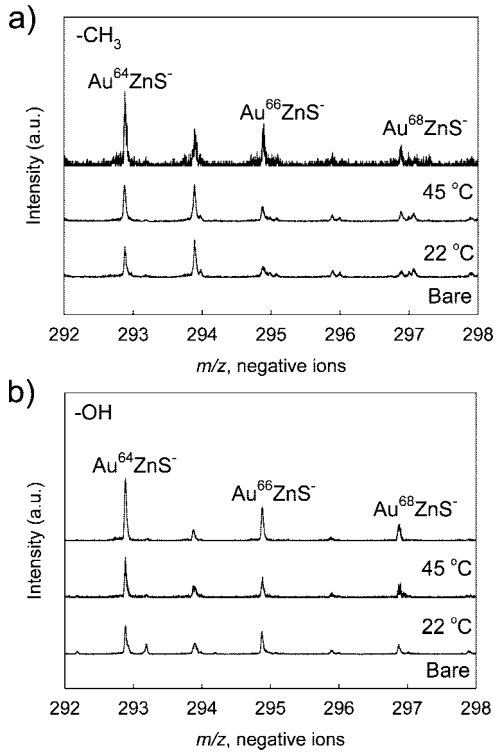

Figure 7. High-resolution negative ion TOF SIMS spectra of $Au^{64}ZnS^-$ (nominal mass $m/z = 293$) for (a) $-CH_3$- and (b) $-OH$-terminated SAMs prior to and after ZnS chemical bath deposition for 2 h at 22 and 45 °C.

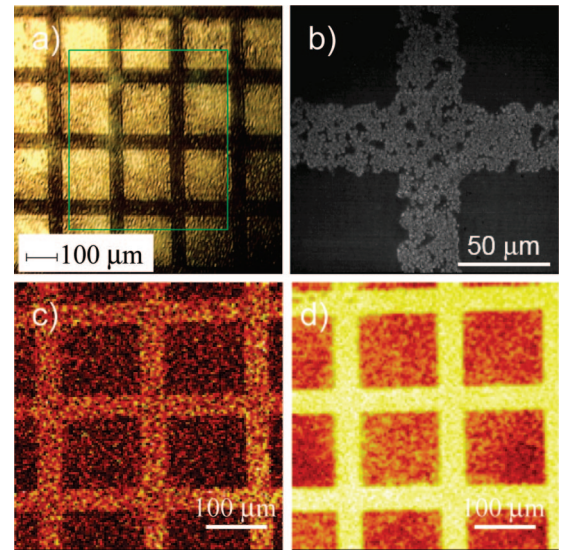

Figure 8. (a) Optical, (b) SEM, and (c,d) TOF SIMS images after ZnS chemical bath deposition on a patterned $-CH_3$/$-COOH$-terminated SAM surface for 15 min at 45 °C. The SEM image indicates that ZnS nanoflowers (light gray) have deposited only in the $-COOH$-terminated SAM areas. The TOF SIMS images are centered at $^{64}Zn^+$ ($m/z = 64$) (c) and OH^- ($m/z = 17$) (d). The OH^- ion intensity is indicative of the $-COOH$-terminated SAM. The intensity of the $^{64}Zn^+$ ion indicates that ZnS has been selectively deposited in the $-COOH$-terminated SAM areas. TOF SIMS analysis: primary ion, Bi^+; kinetic energy = 25 keV; area of analysis = (500 × 500) µm^2, (128 × 128) pixels^2; intensity scale: white = highest number of counts, black = zero counts.

boxylate groups. It is possible that ammonia (or hydrazine) is still bound to the Zn^{2+} upon adsorption to the SAM surface. However, there is no evidence in the SIMS spectra that ammonia (or hydrazine) is present in or on the deposited ZnS films. Once a zinc−SAM complex has formed, it can react with S^{2-} (from the decomposition of thiourea) to form ZnS. This mechanism explains two experimental findings. First, well-separated crystallites form on the $-COOH$-terminated SAMs because the nucleating Zn^{2+}−carboxylate complexes are very sparsely distributed on the surface. The equilibrium constant, K, for the complexation of Zn^{2+} and carboxylic acids is very low (<100).[81] Given the large concentration of ammonium hydroxide and hydrazine present, and the higher binding constants of Zn^{2+} to ammonia ($Zn^{2+} + 4NH_3 \leftrightarrow Zn(NH_3)^{2+}$, $K = 7.9 \times 10^8$) and hydrazine ($Zn^{2+} + 3N_2H_4 \leftrightarrow Zn(N_2H_4)^{2+}$, $K = 3.2 \times 10^5$),[82] it is likely that few surface complexes form. These complexes provide the nucleation sites for ZnS deposition, and therefore discrete ZnS crystallites rather than a smooth ZnS film will tend to grow. When the temperature of the reaction is raised from 22 to 45 °C, the deposition rate does not appear to substantially increase, which was previously identified as characteristic of ion-by-ion growth;[44] the temperature dependence is therefore consistent with the proposed mechanism.

The larger micron-sized crystallites do not strongly adhere to the $-COOH$-, $-OH$-, and $-CH_3$-terminated SAMs and can easily be removed from the surface. TOF SIMS spectra also indicate that there is no interaction between the Zn^{2+} ions and the $-OH$ and $-CH_3$ terminal groups. These observations suggest that ZnS colloids form in solution, aggregate, and adsorb to the surface (cluster-by-cluster deposition). In cluster-by-cluster deposition, the deposition rate increases strongly with temperature,[44,83] which explains the experimentally observed temperature dependence of the reaction for $-OH$- and $-CH_3$-terminated SAMs. At 22 °C, no ZnS deposition is observed on $-OH$- and $-CH_3$-terminated SAMs, whereas at 45 °C, significant deposition is observed.

Finally, we note that a combination of ion-by-ion growth and cluster-by-cluster deposition explains the observed behavior of the micron-sized crystallites during seeded and unseeded growth on $-COOH$- terminated SAMs. For unseeded ZnS growth, cluster-by-cluster deposition dominates due to a lack of nucleating complexes at the surface as argued above. Under seeded growth conditions, the ion-by-ion growth of ZnS nanoflowers is competitive with cluster-by-cluster deposition because preformed Zn^{2+}−carboxylate complexes act as nuclei. Seeding substantially affects the size and distribution of the large crystallites (Figure 5 and Supporting Information), indicating that other growth mechanisms are operative, such as ripening of the large flower-like crystallites. We also note that the seeding process may provide a route for controlling the size of this type of crystallite. However, further work is

needed to investigate the growth mechanisms involved in the formation of large flower-like crystallites.

Nanoflowerbeds: Selective Deposition of ZnS on Patterned SAM Surfaces. These results suggest that under appropriate experimental conditions chemical bath deposition can be employed to selectively deposit ZnS by manipulating the surface chemistry of the substrate. As a demonstration, ZnS CBD was carried out for 15 min on a UV photopatterned $-COOH/-CH_3$-terminared SAM at 45 °C. The sample was sonicated for 5 min in deionized water and then imaged using SEM and TOF SIMS (Figure 8). The images clearly show that ZnS nanoflowers are adsorbed *only* in the $-COOH$-terminated SAM regions (the "bar" areas), while in the $-CH_3$-terminated SAM areas (the "square" areas), no ZnS is adsorbed. Further, using TOF SIMS, we observe $^{64}Zn^+$ (*m/z* 64) (Figure 8c) only in the $-COOH$-terminated SAM areas, indicating that ZnS is present there. No $^{64}Zn^+$ ions are observed in the $-CH_3$-terminated SAM areas.

CONCLUSIONS

We have shown that the chemical bath deposition of ZnS on functionalized SAMs proceeds both by cluster-by-cluster deposition in solution and ion-by-ion growth on the surface. On $-COOH$-terminated SAMs, both ~500 nm nanoflowers and ~2 μm flower-like crystallites are observed. The larger crystallites are deposited from the aggregation of ZnS colloids in solution (cluster-by-cluster deposition) and do not strongly adhere to the surface. In contrast, the ~500 nm nanoflowers are formed *via* an ion-by-ion reaction pathway on the surface and strongly adhere to the surface. These results are consistent with initial formation of $Zn^{2+}-$carboxylate complexes, which act as nucleation sites for the ion-by-ion growth of ZnS.

On $-CH_3$- and $-OH$-terminated SAMs, the dominant growth mechanism is cluster-by-cluster deposition in solution, leading to the deposition of ~2 μm flower-like crystallites which do not strongly adhere to the surface. TOF SIMS data indicate that Zn is present at the Au/S interface after deposition on these SAMS to the Au/S interface.

We have also demonstrated that under the appropriate conditions ZnS can be selectively deposited on patterned $-CH_3/-COOH$-terminated SAM surfaces, creating "nanoflowerbeds".

These results indicate that CBD can be employed to selectively deposit overlayers on organic thin films, and that reaction conditions and surface chemistry may also be used to control the size and morphology of the deposited semiconductor. Further, the data indicate that, for stable overlayers to grow on organic surfaces, surface complexes must first be formed which act as the nucleation sites for further film growth, in agreement with previous gas-phase deposition studies.[77] Since these reactions are selective, patterned SAMs can be employed as templates for the large-area deposition of thin films for applications in photonics, photovoltaics, organic/molecular electronics, and sensing.

METHODS

Materials and Sample Preparation. Gold and chromium were obtained from Alfa Aesar Inc. (Ward Hill, MA) and were of 99.995% purity. Zinc chloride (≥98%), hydrazine hydrate ($N_2H_4 \cdot xH_2O$, $x \sim 1.5$, $N_2H_4 \sim 50-60\%$), thiourea (≥99%), and ammonia hydroxide solution (NH_4OH, 28% in H_2O) were obtained from Sigma Aldrich (Saint Louis, MO). Hexadecanethiol (99%) (HDT) and mercaptohexadecanoic acid (99%) (MHA) were obtained from Asemblon, Inc. (Redmond, WA). All reactants were used without further purification. Mercaptohexadecanol (MHL) was synthesized according to the procedure described by Fisher *et al.*[84]

The preparation of SAMs used in this study has been described in detail previously.[84−87] Briefly, first Cr (~5 nm) and then Au (~100 nm) were thermally deposited onto clean Si native oxide wafers (⟨111⟩, Addison Engineering, Inc., San Jose, CA). The prepared Au substrates were then immersed into a 1 mM ethanolic solution (absolute ethanol, Aaper Alcohol and Chemical Co., Shelbyville, KY) of the relevant hexadecanethiol molecule (with $-CH_3$, $-OH$, $-COOH$ terminal functional groups) for 24 h at ambient temperature (21 ± 2 °C) to prepare well-organized SAMs. The size of the samples used was ~1 × 1 cm^2. To ensure that the prepared SAMs were well-ordered and free from significant chemical contamination, for each batch, one sample was taken and characterized using single-wavelength ellipsometry (Gaertner Scientific Corp., Skokie, IL) and TOF SIMS (ION TOF Inc., Chestnut Hill, NY) prior to chemical bath deposition.

ZnS Chemical Bath Deposition. The plating solution employed in this study consisted of 7.8 mM $ZnCl_2$ (zinc source), 250 mM hydrazine (N_2H_4) (complexing agent), 65 mM ammonia hydroxide (NH_4OH) (complexing agent), and 7.6 mM thiourea (NH_2CSNH_2) (sulfur source). It is noted that the concentration of $ZnCl_2$ and thiourea is lower than typically employed[16,44] and was chosen so that the initial stages of ZnS deposition could be investigated. To make the plating solution, zinc chloride was first dissolved in deionized water, then hydrazine hydrate and ammonia hydroxide solution was added into the solution dropwise. SAM samples were usually immersed in this solution for 15 min before the addition of thiourea (seeding time). After the 15 min seeding time, thiourea was added to the solution to initiate the deposition of ZnS. To investigate the influence of Zn^{2+} complexation with the $-COOH$ terminal group on ZnS deposition, thiourea was added to the bath solution prior to immersion of the MHA SAM (unseeded conditions).

The pH of the bath solution was 10.5 and remained constant throughout the ZnS deposition. Deposition was performed at 22 and 45 °C for times from 1 min to 2 h. After CBD, the samples were rinsed thoroughly with copious amounts of deionized water and absolute ethanol, dried using nitrogen gas, and immediately transferred to the TOF SIMS or SEM for analysis.

UV Photopatterning of SAMs. UV photopatterning of SAMs was performed using the following procedure. First, a mask (a copper TEM grid, Electron Microscopy Inc., Hatfield, PA) was placed on top of the $-COOH$-terminated SAM to be patterned. The sample was then placed approximately 50 mm away from a 500 W Hg arc lamp equipped with a dichroic mirror (to remove IR light) and a narrow-band-pass filter (280−400 nm) (Thermal Oriel, Spectra Physics Inc., Stratford, CT). The $-COOH$-terminated SAM was exposed to UV light for 2 h to ensure complete photooxidation. The UV photopatterned $-COOH$-terminated SAM was then immersed in a freshly made 1 mM ethanolic solution of the second alkanethiol, hexadecanethiol, for 24 h. After the immersion, HDT was adsorbed in the areas exposed to UV light, resulting in a patterned $-COOH/-CH_3$-terminated SAM surface.

The patterned surfaces were rinsed with copious degassed ethanol and dried with N_2 gas.

Time-of-Flight Secondary Ion Mass Spectrometry (TOF SIMS). TOF SIMS analyses were performed using an ION TOF IV spectrometer (ION TOF Inc., Chestnut Hill, NY) equipped with a Bi liquid metal ion gun. Briefly, the apparatus consists of a load lock for sample introduction, preparation and analysis chambers, separated by gate valves. The pressure of the preparation and analysis chambers was maintained at $<3.8 \times 10^{-9}$ mbar. The primary Bi^+ ions were accelerated to 25 keV and contained in a ~100 nm diameter probe beam, and the beam was rastered over a (100 × 100) μm^2 area during spectra acquisition and (500 × 500) μm^2 area during image acquisition. All spectra were acquired within the static regime[88] using a total ion dose less than 10^{11} ions cm^{-2}. The secondary ions were extracted into a time-of-flight mass spectrometer with a 2000 V potential and were re-accelerated to 10 keV before reaching the detector.

The peak intensities were reproducible to within ±10% from scan to scan and from sample to sample. For each ZnS deposition condition, at least two samples were prepared and three areas on each sample were examined. The ion intensity data presented are an average of these measurements.

Three samples of each patterned SAM were prepared, and three spots on each patterned surface were analyzed. The images shown are 500 × 500 μm^2 divided into 128 × 128 pixels.

Optical images of the samples were captured using a video camera (ExwaveHAD, Sony) mounted in the TOF SIMS analysis chamber.

Scanning Electron Microscopy (SEM). SEM measurements were performed on a field emission scanning electron microscope (Hitachi s-4500), equipped with a NORAN Instruments energy dispersive X-ray (EDX) microanalysis system, a back scattering detector, and a mechanical straining stage.

Acknowledgment. The authors acknowledge the financial support of a National Science Foundation grant (Grant No. CHE-058063).

Supporting Information Available: High-resolution negative ion mass spectra of the molecular cluster ion Au_2M^- (M = $-S(CH_2)_{15}X$; X = −COOH, $-CH_3$, and −OH) prior to and after ZnS CBD for 2 h at 22 and 45 °C; positive and negative ion mass spectra of −COOH-, $-CH_3$-, and −OH-terminated SAMs to prior to and after ZnS CBD for 2 h at 22 and 45 °C; SEM images after ZnS CBD on −COOH-terminated SAM at 45 °C under "unseeded" conditions for immersion times from 1 to 120 min; size distributuins and average diameters of the large flower-like crystallites for ZnS CBD under seeded and unseeded experimental conditions on −COOH-terminated SAM at 45 °C for immersion times from 1 to 120 min. This material is available free of charge *via* the Internet at http://pubs.acs.org.

REFERENCES AND NOTES

1. Hu, J.; Odom, T. W.; Lieber, C. M. Chemistry and Physics in One Dimension: Synthesis and Properties of Nanowires and Nanotubes. *Acc. Chem. Res.* **1999**, *32*, 435–445.
2. Gao, X. D.; Li, X. M.; Yu, W. D. Morphology and Optical Properties of Amorphous ZnS Films Deposited by Ultrasonic-Assisted Successive Ionic Layer Adsorption and Reaction Method. *Thin Solid Films* **2004**, *468*, 43–47.
3. Ruffner, J. A.; Himel, M. D.; Mizrahi, V.; Stegeman, G. I.; Gibson, U. J. Effects of Low Substrate Temperature and Ion Assisted Deposition on Composition, Optical Properties, and Stress of ZnS Thin Films. *Appl. Opt.* **1989**, *28*, 5209–5214.
4. Horii, Y.; Kitagawa, M.; Taneoka, H.; Kusano, H.; Murakami, T.; Hino, Y.; Kobayashi, H. Electroluminescence Properties of PVCz Electroluminescent Devices Doped with Nano-Crystalline Particles. *Mater. Sci. Eng. B* **2001**, *85*, 92–95.
5. Que, W.; Zhou, Y.; Lam, Y. L.; Chan, Y. C.; Kam, C. H.; Liu, B. W.; Gan, L. M.; Chew, C. H.; Xu, G. Q.; Chua, S. J.; *et al.* Photoluminescence and Electroluminescence from Copper Doped Zinc Sulphide Nanocrystals/Polymer Composite. *Appl. Phys. Lett.* **1998**, *73*, 2727–2729.
6. Kakuta, N.; Park, K. H.; Finlayson, M. F.; Ueno, A.; Bard, A. J.; Campion, A.; Fox, M. A.; Webber, S. E.; White, J. M. Photoassisted Hydrogen Production Using Visible Light and Coprecipitated ZnS · CdS Without a Noble Metal. *J. Phys. Chem.* **1985**, *89*, 732–734.
7. Johne, P.; Kisch, H. Photoreduction of Carbon Dioxide Catalysed by Free and Supported Zinc and Cadmium Sulphide Powders. *J. Photochem. Photobiol., A* **1997**, *111*, 223–228.
8. Hu, J.-S.; Ren, L.-L.; Guo, Y.-G.; Liang, H.-P.; Cao, A.-M.; Wan, L.-J.; Bai, C.-L. Mass Production and High Photocatalytic Activity of ZnS Nanoporous Particles. *Angew. Chem., Int. Ed.* **2005**, *44*, 1269–1273.
9. Ledger, A. M. Inhomogeneous Interface Laser Mirror Coatings. *Appl. Opt.* **1979**, *18*, 2979–2989.
10. Katayama, H.; Oda, S.; Kukimoto, H. ZnS Blue-Light-Emitting Diodes with an External Quantum Efficiency of 5 × 10^{-4}. *Appl. Phys. Lett.* **1975**, *27*, 697–699.
11. Lawther, C.; Fujita, T.; Takagi, T. Blue-Emitting S^+-Implanted An-ZnS Schottky Barrier Diodes. *Jpn. J. Appl. Phys.* **1980**, *19*, 939–947.
12. Taguchi, T.; Yokogawa, T. Effects of Oxygen Impurity on the Surface in ZnS Crystals and Blue Light-Emitting Diodes. *J. Phys. D: Appl. Phys.* **1984**, *17*, 1067–1082.
13. Ohno, T.; Kurisu, K.; Taguchi, T. Growth of High-Quality Cubic ZnS Crystals and Their Application to MIS Blue Light-Emitting Diodes. *J. Cryst. Growth* **1990**, *99*, 737–742.
14. Yamaga, S. Epitaxial ZnS MπS Blue Light Emitting Diode Fabricated on n^+-GaAs by Low-Pressure Metalorganic Vapor Phase Epitaxy. *Jpn. J. Appl. Phys.* **1991**, *30*, 437–441.
15. Yamaga, S. ZnS as Blue LED. *Jpn. J. Appl. Phys.* **1991**, *30*, 437.
16. Ben Nasr, T.; Kamoun, N.; Kanzari, M.; Bennaceur, R. Effect of pH on the Properties of ZnS Thin Films Grown by Chemical Bath Deposition. *Thin Solid Films* **2006**, *500*, 4–8.
17. Nakada, T.; Mizutani, M. 18% Efficiency Cd-Free Cu(In, Ga)Se_2 Thin-Film Solar Cells Fabricated Using Chemical Bath Deposition (CBD)-ZnS Buffer Layers. *Jpn. J. Appl. Phys.* **2002**, *41*, L165–L167.
18. Huang, K. J.; Rajendran, P.; Liddell, C. M. Chemical Bath Deposition Synthesis of Sub-Micron ZnS-Coated Polystyrene. *J. Colloid Interface Sci.* **2007**, *308*, 112–120.
19. Huang, J. M.; Yang, Y.; Yang, B.; Liu, S. Y.; Shen, J. C. Assembly and Applications of the Inorganic Nanocrystals in Polymer Networks. *Thin Solid Films* **1998**, *327−329*, 536–540.
20. Tonouchi, M.; Sun, Y.; Miyasato, T.; Sakama, H.; Ohmura, M. Room-Temperature Synthesis of ZnS:Mn Films by H_2 Plasma Chemical Sputtering. *Jpn. J. Appl. Phys.* **1990**, *29*, L2453–L2456.
21. Wang, Y.; Zhang, L.; Liang, C.; Wang, G.; Peng, X. Catalytic Growth and Photoluminescence Properties of Semiconductor Single-Crystal ZnS Nanowires. *Chem. Phys. Lett.* **2002**, *357*, 314–318.
22. Zhu, Y.-C.; Bando, Y.; Xue, D.-F. Spontaneous Growth and Luminescence of Zinc Sulfide Nanobelts. *Appl. Phys. Lett.* **2003**, *82*, 1769–1771.
23. Yoneta, M.; Ohishi, M.; Saito, H.; Hamasaki, T. Low Temperature Molecular Beam Epitaxial Growth of ZnS/GaAs(001) by Using Elemental Sulfur Source. *J. Cryst. Growth* **1993**, *127*, 314–317.
24. Afifi, H. H.; Mahmoud, S. A.; Ashour, A. Structural Study of ZnS Thin Films Prepared by Spray Pyrolysis. *Thin Solid Films* **1995**, *263*, 248–251.
25. Elidrissi, B.; Addoua, M.; Regraguia, M.; Bougrinea, A.; Kachouanea, A.; Bernède, J. C. Structure, Composition and Optical Properties of ZnS Thin Films Prepared by Spray Pyrolysis. *Mater. Chem. Phys.* **2001**, *68*, 175–179.
26. Hillie, K. T.; Curren, C.; Swart, H. C. ZnS Thin Films Grown on Si(100) by XeCl Pulsed Laser Ablation. *Appl. Surf. Sci.* **2001**, *177*, 73–77.
27. Dean, P. J.; Pitt, A. D.; Skolnick, M. S.; Wright, P. J.; Cockayne, B. Optical Properties of Undoped Organometallic Grown ZnSe and ZnS. *J. Cryst. Growth* **1982**, *59*, 301–306.

28. Nakamura, S.; Yamada, Y.; Taguchi, T. Room-Temperature 340 nm Ultraviolet Electroluminescence from ZnS-Based Light-Emitting Diodes. *J. Cryst. Growth* **2000**, *214/215*, 1091–1095.
29. Abounadi, A.; Di Blasio, M.; Bouchara, D.; Calas, J.; Averous, M.; Briot, O.; Briot, N.; Cloitre, T.; Aulombard, R. L.; Gil, B. Reflectivity and Photoluminescence Measurements in ZnS Epilayers Grown by Metal-Organic Chemical-Vapor Deposition. *Phys. Rev. B* **1994**, *50*, 11677–11683.
30. Tammenmaa, M.; Koskinen, T.; Hiltunen, L.; Niinistö, L.; Leskelä, M. Zinc Chalcogenide Thin Films Grown by the Atomic Layer Epitaxy Technique Using Zinc Acetate as Source Material. *Thin Solid Films* **1985**, *124*, 125–128.
31. Lokhande, C. D.; Jadhav, M. S.; Pawar, S. H. Electrodeposition of ZnS Films from an Alkaline Bath. *J. Electrochem. Soc.* **1989**, *136*, 2756–2757.
32. Sanders, B. W.; Kitai, A. H. The Electrodeposition of Thin Film Zinc Sulphide from Thiosulphate Solution. *J. Cryst. Growth* **1990**, *100*, 405–410.
33. Fathy, N.; Kobayashi, R.; Ichimura, M. Preparation of ZnS Thin Films by the Pulsed Electrochemical Deposition. *Mater. Sci. Eng. B* **2004**, *107*, 271–276.
34. Meldrum, F. C.; Flath, J.; Knoll, W. Formation of Patterned PbS and ZnS Films on Self-Assembled Monolayers. *Thin Solid Films* **1999**, *348*, 188–195.
35. O'Brien, P.; McAleese, J. Developing an Understanding of the Processes Controlling the Chemical Bath Deposition of ZnS and CdS. *J. Mater. Chem.* **1998**, *8*, 2309–2314.
36. Roy, P.; Ota, J. R.; Srivastava, S. K. Crystalline ZnS Thin Films by Chemical Bath Deposition Method and its Characterization. *Thin Solid Films* **2006**, *515*, 1912–1917.
37. Yamaguchi, K.; Yoshida, T.; Lincot, L.; Minoura, H. Mechanistic Study of Chemical Deposition of ZnS Thin Films from Aqueous Solutions Containing Zinc Acetate and Thioacetamide by Comparison with Homogeneous Precipitation. *J. Phys. Chem. B* **2003**, *107*, 387–397.
38. Lee, J.; Lee, S. H.; Cho, S.; Kim, S.; Park, I. Y.; Choi, Y. D. Role of Growth Parameters on Structural and Optical Properties of ZnS Nanocluster Thin Films Grown By Solution Growth Techniques. *Mater. Chem. Phys.* **2002**, *77*, 254–260.
39. O'Brien, P.; Otway, D. J.; Smyth-Boyle, D. The Importance of Ternary Complexes in Defining Basic Conditions for the Deposition of ZnS by Aqueous Chemical Bath Deposition. *Thin Solid Films* **2000**, *361−362*, 17–21.
40. Sartale, S. D.; Sankapal, B. R.; Lux-Steiner, M.; Ennaoui, A. Preparation of Nanocrystalline ZnS by a New Chemical Bath Deposition Route. *Thin Solid Films* **2005**, *480−481*, 168–172.
41. Bayer, A.; Boyle, D. S.; O'Brien, P. *In Situ* Studies of the Chemical Bath Deposition of Zinc Sulfide from Acidic Solutions. *J. Mater. Chem.* **2002**, *12*, 2940–2944.
42. Cruz-Vázquez, C.; Rocha-Alonzo, F.; Burruel-Ibarra, S. E.; Barboza-Flores, M.; Bernal, R.; Inoue, M. A New Chemical Bath Deposition Method for Fabricating ZnS, $Zn(OH)_2$, and ZnO Thin Films, and the Optical and Structural Characterization of These Materials. *Appl. Phys. A* **2004**, *79*, 1941–1945.
43. Lădar, M.; Popovici, E.-J.; Baldea, I.; Grecu, R.; Indrea, E. Studies on Chemical Bath Deposited Zinc Sulphide Thin Films with Special Optical Properties. *J. Alloys Compd.* **2007**, *434−435*, 697–700.
44. Doña, J. M.; Herrero, J. Process and Film Characterization of Chemical-Bath-Deposited ZnS Thin Films. *J. Electrochem. Soc.* **1994**, *141*, 205–210.
45. Doña, J. M.; Herrero, J. Chemical Bath Codeposited CdS-ZnS Film Characterization. *Thin Solid Films* **1995**, *268*, 5–12.
46. Gŏde, F.; Gümüş, C.; Zor, M. Influence of the Thickness on Physical Properties of Chemical Bath Depositied Hexagonal ZnS Thin Films. *J. Optoelectron. Adv. Mater.* **2007**, *9*, 2186−2191.
47. Cheng, J.; Fan, D. B.; Wang, H.; Liu, B. W.; Zhang, Y. C.; Yan, H. Chemical Bath Deposition of Crystalline ZnS Thin Films. *Semicond. Sci. Technol.* **2003**, *18*, 676–679.
48. Ulman, A. Formation and Structure of Self-Assembled Monolayers. *Chem. Rev.* **1996**, *96*, 1533–1554.
49. Schreiber, F. Structure and Growth of Self-Assembling Monolayers. *Prog. Surf. Sci.* **2000**, *65*, 151–256.
50. Tarlov, M. J.; Burgess, D. R. F., Jr.; Gillen, G. UV Photopatterning of Alkanethiolate Monolayers Self-Assembled on Gold and Silver. *J. Am. Chem. Soc.* **1993**, *115*, 5305–5306.
51. Cooper, E.; Leggett, G. J. Influence of Tail-Group Hydrogen Bonding on the Stabilities of Self-Assembled Monolayers of Alkylthiols on Gold. *Langmuir* **1999**, *15*, 1024–1032.
52. Brewer, N. J.; Rawsterne, R. E.; Kothari, S.; Leggett, G. J. Oxidation of Self-Assembled Monolayers by UV Light with a Wavelength of 254 nm. *J. Am. Chem. Soc.* **2001**, *123*, 4089–4090.
53. Zhou, C.; Walker, A. V. UV Photooxidation and Photopatterning of Alkanethiolate Self-Assembled Monolayers Adsorbed on GaAs (001). *Langmuir* **2007**, *23*, 8876–8881.
54. Smith, R. K.; Lewis, P. A.; Weiss, P. S. Patterning Self-Assembled Monolayers. *Prog. Surf. Sci.* **2004**, *75*, 1–68.
55. Gates, B. D.; Xu, Q.; Stewart, M.; Ryan, D.; Wilson, C. G.; Whitesides, G. M. New Approaches to Nanofabrication: Molding, Printing, and Other Techniques. *Chem. Rev.* **2005**, *105*, 1171–1196.
56. Lercel, M. J.; Craighead, H. G.; Parikh, A. N.; Seshadri, K.; Allara, D. L. Sub-10nm Lithography with Self-Assembled Monolayers. *Appl. Phys. Lett.* **1996**, *68*, 1504–1506.
57. Whelan, C. S.; Lercel, M. J.; Craighead, H. G.; Seshadri, K.; Allara, D. L. Improved Electron-Beam Patterning of Si with Self-Assembled Monolayers. *Appl. Phys. Lett.* **1996**, *69*, 4245–4247.
58. Chen, J.; Lee, T.; Su, J.; Wang, W.; Reed, M. A.; Rawlett, A. M.; Kozaki, M.; Yao, Y.; Jagessar, R. C.; Dirk, S. M. *et al.* Molecular Electronic Devices. In *Molecular Nanoelectronics*; Reed, M. A., Lee, T., Eds.; American Scientific Publishers: Stevenson Ranch, CA, 2003; pp 40−114.
59. Love, J. C.; Estroff, L. A.; Kriebel, J. K.; Nuzzo, R. G.; Whitesides, G. M. Self-Assembled Monolayers of Thiolates on Metals as a Form of Nanotechnology. *Chem. Rev.* **2005**, *105*, 1103–1169.
60. Davis, F.; Higson, S. P. J. Structured Thin Films as Functional Components Within Biosensors. *Biosens. Bioelectron.* **2005**, *21*, 1–20.
61. Young, R. A. Biomedical Discovery with DNA Arrays. *Cell* **2000**, *102*, 9–15.
62. Flink, S.; van Veggel, F. C. J. M.; Reinhoudt, D. N. Sensor Functionalities in Self-Assembled Monolayers. *Adv. Mater.* **2000**, *12*, 1315–1328.
63. Abbott, N. L.; Rolison, D. R.; Whitesides, G. M. Combining Micromachingin and Molecular Self-Assembly to Fabricate Microelectrodes. *Langmuir* **1994**, *10*, 2672–2682.
64. Mrksich, M.; Whitesides, G. M. Using Self-Assembled Monolayers to Understand the Interactionsof Man-Made Surfaces with Proteins and Cells. *Annu. Rev. Biophys. Biomol. Struct.* **1996**, *25*, 55–78.
65. Weibel, D. B.; DiLuzio, W. R.; Whitesides, G. M. Microfabrication Meets Microbiology. *Nat. Rev. Microbiol.* **2007**, *5*, 209–218.
66. Kumar, A.; Biebuyck, H. A.; Whitesides, G. M. Patterning Self-Assembled Monolayers: Applications in Materials Science. *Langmuir* **1994**, *10*, 1498–1511.
67. Calvert, J. M.; Georger, J. H.; Schnur, J. M.; Schoen, P. E.; Peckerar, M. C.; Pehrsson, P. E. Deep UV Photochemistry and Patterning of Self-Assembled Monolayer Films. *Thin Solid Films* **1992**, *210/211*, 359–363.
68. Jeon, N. L.; Nuzzo, R. G.; Xia, Y.; Mrksich, M.; Whitesides, G. M. Patterned Self-Assembled Monolayers Formed by Microcontact Printing Direct Selective Metallization by Chemical Vapor Deposition on Planar and Nonplanar Substrates. *Langmuir* **1995**, *11*, 3024–3026.
69. Schoer, J. K.; Ross, C. B.; Crooks, R. M.; Corbitt, T. S.; Hampden-Smith, M. J. Scanning Probe Lithography. 2. Selective Chemical Vapor Deposition of Copper into Scanning Tunneling Microscope-Defined Patterns. *Langmuir* **1994**, *10*, 615–618.

70. Jeon, N. L.; Clem, P. G.; Payne, D. A.; Nuzzo, R. G. A Monolayer-Based Lift-Off Process for Patterning Chemical Vapor Deposition Copper Thin Films. *Langmuir* **1996**, *12*, 5350–5355.
71. Jeon, N. L.; Lin, W.; Erhardt, M. K.; Girolami, G. S.; Nuzzo, R. G. Selective Chemical Vapor Deposition of Platinum and Palladium Directed by Monolayers Patterned Using Microcontact Printing. *Langmuir* **1997**, *13*, 3833–3838.
72. Jeon, N. L.; Clem, P. G.; Nuzzo, R. G.; Payne, D. A. Patterning of Dielectric Oxide Thin Layers by Microcontact Printing of Self-Assembled Monolayers. *J. Mater. Res.* **1995**, *10*, 2996–2999.
73. Bunker, B. C.; Rieke, P. C.; Tarasevich, B. J.; Campbell, A. A.; Fryxell, G. E.; Graff, G. L.; Song, L.; Liu, J.; Virden, J. W.; McVay, G. L. Ceramic Thin-Film Formation on Functionalized Interfaces Through Biomimetic Processing. *Science* **1994**, *264*, 48–55.
74. Rieke, P. C.; Tarasevich, B. J.; Wood, L. L.; Engelhard, M. H.; Baer, D. R.; Fryxell, G. E.; John, C. M.; Laken, D. A.; Jaehnig, M. C. Spatially Resolved Mineral Deposition on Patterned Self-Assembled Monolayers. *Langmuir* **1994**, *10*, 619–622.
75. Dressick, W. J.; Dulcey, C. S.; Georger, J. H., Jr.; Calvert, J. M. Photopatterning and Selective Electroless Metallization of Surface-Attached Ligands. *Chem. Mater.* **1993**, *5*, 148–150.
76. Zhou, C.; Nagy, G.; Walker, A. V. Towards Molecular Electronic Circuitry: Selective Deposition of Metals on Patterned Self-Assembled Monolayer Surfaces. *J. Am. Chem. Soc.* **2005**, *127*, 12160–12161.
77. Lu, P.; Demirkan, K.; Opila, R. L.; Walker, A. V. Room Temperature Chemical Vapor Deposition of Aluminum and Aluminum Oxides on Alkanethiolate Self-Assembled Monolayers. *J. Phys. Chem. C* **2008**, *112*, 2091–2098.
78. Dronavajjala, K. D.; Rajagopalan, R.; Uppili, S.; Sen, A.; Allara, D. L.; Foley, H. C. A Simple Technique to Grow Polymer Brushes Using *In Situ* Surface Ligation of an Organometallic Initiator. *J. Am. Chem. Soc.* **2006**, *128*, 13040–13041.
79. Froment, M.; Lincot, L. Phase Formation Processes in Solution at the Atomic Level: Metal Chalcogenide Semiconductors. *Electrochim. Acta* **1995**, *40*, 1293–1303.
80. Kanicky, J. R.; Shah, D. O. Effect of Degree, Type, and Position of Unsaturation on the pK_a of Long-Chain Fatty Acids. *J. Colloid Interface Sci.* **2002**, *256*, 201–207.
81. Martell, A. E.; Smith, R. M. *Critical Stability Constants*; Plenum Press: New York, 1974; Vol. 3, pp 1−12.
82. Smith, R. M.; Martell, A. E. *Critical Stability Constants*; Plenum Press: New York, 1976; Vol. 4, pp 40−43.
83. Doña, J. M.; Herrero, J. Chemical Bath Deposition of CdS Thin Films: Electrochemical *In Situ* Kinetic Studies. *J. Electrochem. Soc.* **1992**, *139*, 2810–2814.
84. Fisher, G. L.; Walker, A. V.; Hooper, A. E.; Tighe, T. B.; Bahnck, K. B.; Skriba, H. T.; Reinard, M. D.; Haynie, B. C.; Opila, R. L.; Winograd, N.; *et al.* Bond Insertion, Complexation, and Penetration Pathways of Vapor-Deposited Aluminum Atoms with HO- and CH_3O-Terminated Organic Monolayers. *J. Am. Chem. Soc.* **2002**, *124*, 5528–5541.
85. Nuzzo, R. G.; Dubios, L. H. L. A. D. Fundamental Studies of Microscopic Wetting on Organic Surfaces. 1. Formation and Structural Characterization of a Self-Consistent Series of Polyfunctional Organic Monolayers. *J. Am. Chem. Soc.* **1990**, *112*, 558–569.
86. Hooper, A. E.; Fisher, G. L.; Konstadinidis, K.; Jung, D. R.; Nguyen, H.; Opila, R. L.; Collins, R. W.; Winograd, N.; Allara, D. L. Chemical Effects of Methyl and Methyl Ester Groups on the Nucleation and Growth of Vapor-Deposited Aluminum Films. *J. Am. Chem. Soc.* **1999**, *121*, 8052–8064.
87. Fisher, G. L.; Hooper, A. E.; Opila, R. L.; Allara, D. L.; Winograd, N. The Interaction of Vapor-Deposited Al Atoms with CO_2H Groups at the Surface of a Self-Assembled Alkanethiolate Monolayer on Gold. *J. Phys. Chem. B* **2000**, *104*, 3267–3273.
88. Vickerman, J. C. ToF-SIMS -An Overview. In *ToF-SIMS: Surface Analysis by Mass Spectrometry*; Vickerman, J. C., Briggs, D., Eds.; IM Publications and Surface Spectra Limited: Chichester and Manchester, UK, 2001; pp 1−40.